Research Article Vol. 32, No. 12 / 3 Jun 2024 / Optics Express 20459
Optics EXPRESS

Transient gas-induced differential refractive index effects in as-drawn hollow core optical fibers

THOMAS W. KELLY,[1,4] SHUICHIRO RIKIMI,[1,5] IAN A. DAVIDSON,[1] YONG CHEN,[1,2] SIMON BAWN,[2] THOMAS D. BRADLEY,[1,3] AUSTIN A. TARANTA,[1] FRANCESCO POLETTI,[1] DAVID J. RICHARDSON,[1,2] PETER HORAK,[1] AND NATALIE V. WHEELER[1]

[1]*Optoelectronics Research Centre, Zepler Institute, University of Southampton, Southampton SO17 1BJ, UK*
[2]*Microsoft Azure, Unit 7, The Quadrangle, Premier Way, Romsey, USA*
[3]*Now at the High-Capacity Optical Transmission Laboratory, Eindhoven University of Technology, 5600 MB, Netherlands*
[4]*T.W.Kelly@soton.ac.uk*
[5]*rikirikiusausa@gmail.com*

Abstract: When a hollow core fiber is drawn, the core and cladding holes within the internal cane geometry are pressurized with an inert gas to enable precise control over the internal microstructure of the fiber and counteract surface tension forces. Primarily by considering the temperature drop as the fiber passes through the furnace and the geometrical transformation of the internal microstructure from preform-to-fiber, we recently established that the gas pressure within the final 'as-drawn' fiber is substantially below atmospheric pressure. We have also established that slight changes in the gas refractive index within the core and surrounding cladding holes induced by changes in gas pressure are sufficient to significantly affect both the modality and loss of the fiber. Here we demonstrate, through both simulations and experimental measurements, that the combination of these effects leads to transient changes in the fiber's attenuation when the fibers are opened to atmosphere post-fabrication. It is important to account for this phenomenon for accurate fiber characterization, particularly when long lengths of fiber are drawn where it could take many weeks for every part of the internal microstructure to reach atmospheric pressure.

1. Introduction

The development of hollow core optical fibers (HCFs), in which light can be transmitted with low loss in a gas-filled core, has progressed rapidly in recent years [1]. The minimum losses achieved using advanced HCF designs are now competitive with standard silica fiber technology across all key wavelengths from the UV [2,3], visible to the mid-infrared [4–6]. This, combined with the ultralow non-linearity and low latency offered by a HCF, means that we have now reached a point where these specialty fibers are being deployed in commercial applications, including telecommunications [7,8]. As such, factors such as the consistency of optical performance and long-term reliability [9] are becoming increasingly important.

In a HCF, the central hollow core, where light is transmitted, is surrounded by a carefully designed microstructured cladding. This cladding consists of several further air holes which are defined by thin glass (usually silica) membranes. Both the central hollow core and the surrounding cladding holes run along the full fiber length. While key outstanding optical properties of HCFs

#517755 https://doi.org/10.1364/OE.517755
Journal © 2024 Received 5 Jan 2024; revised 24 Apr 2024; accepted 6 May 2024; published 20 May 2024

Optics EXPRESS

are enabled by light transmission in a gas-filled core, this feature also potentially adds extra complexity when considering the consistency of the optical performance.

For applications such as gas sensing and non-linear photonics, where short lengths of fiber are typically used, the internal gas composition inside of the fiber is actively controlled and well known [10]. However, little attention has been paid to unintentional gas species within these fibers, whose absorption bands will increase the fiber's attenuation over specific wavelength ranges [11,12], whether this be in the near-IR or the so-called mid-IR 'fingerprint' region. The presence of these gases is important to consider for various deployment scenarios. We previously reported on the evolution of the concentration of atmospheric gas species (e.g., water vapor, carbon dioxide, oxygen, nitrogen) inside HCFs using several spectroscopic methods [13,14] and concluded that these species can originate from the ingress of external atmospheric gas species when the ends of the fiber are left open post-fabrication. We believe that this is largely facilitated by pressure-driven flow because of the lower (sub-atmospheric) pressure inside of the HCF after fabrication. This low pressure is mostly due to the temperature drop during fabrication from the furnace (at ~2000°C) to room temperature, which causes a corresponding drop in gas pressure inside the fiber [14].

Additionally, we have shown that a difference in gas pressure between the core and cladding holes of an antiresonant HCF can significantly affect the fiber's optical properties by altering the relative effective refractive indices of the propagating modes in different parts of the microstructure. This is because the pressure difference creates a gas-induced differential refractive index (GDRI) between the core and cladding regions [15]. Hence, when considering the consistency of the optical performance of a HCF, in conjunction with the low 'as-drawn' pressure, it is important to consider potential changes in the gas composition and pressure within different parts of the fiber microstructure.

In this paper, we describe transient changes in the optical properties of HCFs post-fabrication due to a combination of the low 'as-drawn' internal pressure and GDRI. We continually measure the transmission of a single-cladding ring ("tubular") hollow core antiresonant fiber (HC-ARF) whose ends are opened post-fabrication. A simple one-dimensional model (Hagen-Pouiselle flow) is used to calculate gas pressure changes within the HCF's microstructure due to the low 'as-drawn' pressure and in conjunction with finite element method (FEM) analysis to solve for the fiber modes, the expected change in confinement loss is also calculated. Further measurements are carried out with a state-of-the-art nested antiresonant nodeless fiber (NANF). We demonstrate a good agreement between experiment and simulations which supports our hypothesis that transient changes in the internal gas pressure of HCFs post-fabrication can change the optical performance of the fiber. The magnitude of these changes is dependent on several factors, including fiber design, length, and operating wavelength, and it is critical to consider this effect to enable accurate optical characterization and consistent optical performance over time.

2. Gas-flow dynamics in as-drawn HCFs

The HCFs used in this paper were all fabricated in-house by the conventional two-stage stack and draw technique. For the first experiments reported here, we use a tubular design, single-cladding ring, antiresonant HCF. In fabrication, seven identical capillary tubes which form the cladding are assembled into a jacket tube to form the initial preform, which is then drawn down in two stages to the final fiber. During both drawing stages, the preform is heated to a temperature of ~ 2000 °C to reduce the silica glass viscosity, and in the second drawing stage a preform with a diameter of a few millimeters is drawn to the final fiber diameter (~ 200 µm). A comprehensive study into the draw-down dynamics can be found in [16].

Figure 1(a). shows the fiber structure. This design was chosen for this study as it has a relatively simple cladding structure compared to more advanced HC-ARFs (see e.g., NANF [4], conjoined-tube fibers [17]). This simpler structure aids the gas flow modelling process. The fiber

Optics EXPRESS

core, with a diameter of 18.6 µm, is surrounded by a cladding composed of seven tubes with an average inner diameter and membrane thickness of 9.3 µm and ~ 440 nm respectively. Note, the fiber's core size is defined using the largest circle that can be inscribed in the core region which just touches the outer surfaces of the cladding membranes (yellow dashed line in Fig. 1(a)).

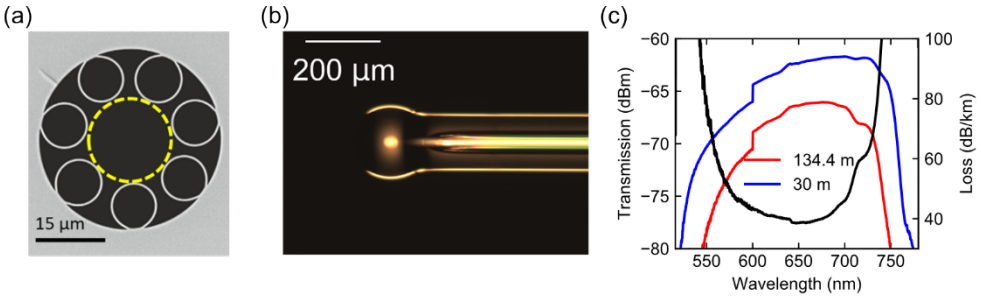

Fig. 1. (a) Scanning electron microscope image of the cross-section of the tubular HC-ARF used; the yellow dashed line indicates the definition of the core region used in the gas flow simulations; (b) Microscope image of the end of a tubular HC-ARF, where the core and cladding holes have been sealed to eliminate gas flow between the holes in the fiber and the external environment. (c) Cutback measurement of the tubular fiber; transmission through 134.4 m and 30 m (red and blue lines respectively) and calculated loss (black line).

To precisely control the wall thickness of the capillaries and the size of the hollow core, the core and cladding holes in the preform are separately pressurized during the fiber draw with an inert gas. The core pressure applied during fabrication was 0.5 kPa + 1 atm. In [14], the pressure inside a fabricated fiber is estimated by using the ideal gas law and considering the drop in temperature of a small section of the fiber exiting the furnace immediately after the neck-down at ~1400 °C to a similar section of fiber just outside of the furnace at room temperature. Following this approach, we estimate the internal gas pressure within our fiber to be ~18 kPa (~0.2 atm) immediately after fabrication. Although this estimation simplifies the complex gas flow dynamics during the draw, the change in temperature in combination with the increased air filling fraction of the final fiber compared to the original preform provides key driving factors behind the initial low pressure inside a HCF. To preserve the initial composition and pressure of the gas inside the core and cladding holes post-fabrication, the ends of the fiber were sealed using an arc-fusion splicer immediately after fabrication as shown in Fig. 1(b). We refer to these sealed fibers under a partial vacuum as 'as-drawn' fiber. Figure 1(c) shows the measured cutback spectrum of the tubular fiber. The fiber ends were cleaved more than two weeks prior to taking the cutback measurement. This was a sufficient amount of time to ensure that all parts of the internal microstructure had reached atmospheric pressure and that there was no variation in the loss between measuring the transmission of the long and short section of fiber.

As the internal gas pressure is substantially below atmospheric pressure, we would expect that when the 'as-drawn' sample is un-sealed, pressure-driven gas flow will push air into the core and cladding holes of the fiber until the internal pressure equalizes with that of the surrounding environment. The dynamics of pressure-driven gas flow in HCFs have been studied and reported in several papers (see e.g., [18–20]). By modifying the diffusion equation for pressure-driven flow in the hydrodynamic regime using Hagen-Poiseuille flow, the pressure inside the fiber as a function of time and position can be obtained by numerically solving the following [18]

$$\frac{\partial P}{\partial t} = \frac{r^2}{8\mu}\frac{\partial}{\partial x}\left(P\frac{\partial P}{\partial x}\right), \tag{1}$$

Optics EXPRESS

where P, r, μ, t and x are the pressure, the hole radius, the dynamic viscosity, the time, and the axial position along the fiber, respectively. Equation (1) shows that the change in pressure inside the fiber scales with r^2, hence when considering filling times in a HCF, the hole radius will be a critical factor. Based on this and considering the fiber in Fig. 1(a), we would expect the core to fill ~ 4 times faster than the cladding holes, leading to transient pressure differences between the core and cladding regions.

Equation (1) is formulated under the assumption of a circular bore. To apply this one-dimensional model to our HCF, we approximate the core as a circular capillary equal to the core radius (as indicated in Fig. 1(a)). To match experimental conditions discussed later, we model a 36.75 m long fiber, being filled from both ends with air at standard temperature and pressure, and with viscosity, $\mu = 1.82 \times 10^{-5}$ kg/(m.s) [21]. Through the arguments presented above we assume that the initial pressure inside our as-drawn sample to be 18 kPa.

Figure 2(a) shows the calculated spatial variation of the normalized pressure as a function of the position at times: 0.6, 1.5 and 5.8 hours after un-sealing the fiber ends for a capillary equal to the core radius in the upper graph and a capillary equal to the average cladding tube inner radius in the lower graph. Figure 2(b) shows the average pressure in the core and cladding as a function of time, as found by integrating the pressure distribution along the fiber length; as expected the core pressure increases faster. The blue curve shows the differential pressure that therefore exists between the core and cladding ($\Delta P = P_{core} - P_{cladd}$) due to the different filling rates of the respective regions; this reaches a maximum approximately 1.5 hours after the fiber ends are unsealed, before gradually decreasing until the core and cladding pressures equalize after ~ 15 hours. The existence of this pressure transient can alter the degree of coupling between the guided core modes and surrounding lossy modes in the cladding tubes since the pressure induced change in the refractive index of the gas alters the difference in phase constants between these modes [15].

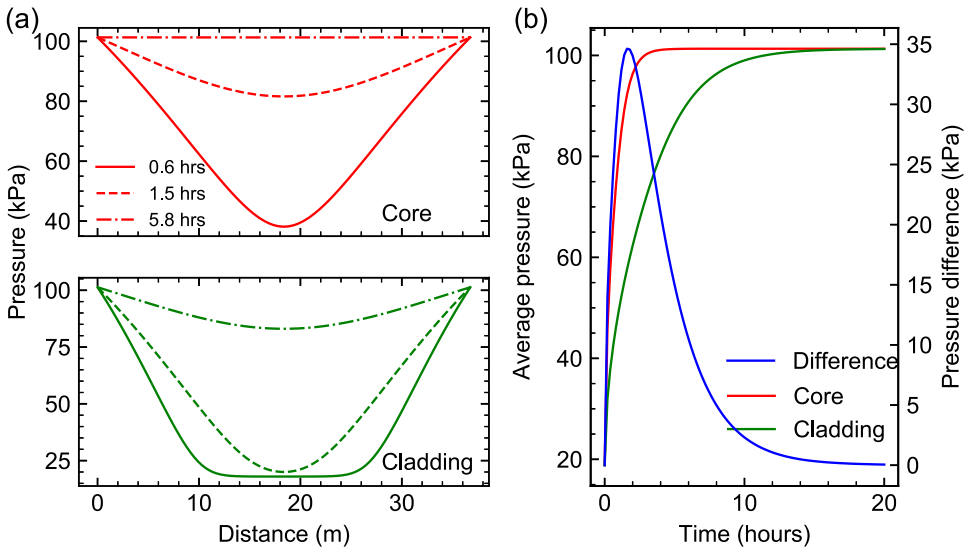

Fig. 2. (a) Simulated gas pressure distributions along a 36.75 m length of tubular HC-ARF at three different times after opening an as-drawn sample to atmospheric pressure for the fiber's core (top panel) and a cladding hole (lower panel) assuming an initial pressure of 18 kPa in the core and cladding holes; (b) simulated average pressure in the core (red line) and the cladding (green line) as a function of time and calculated pressure difference (ΔP) between the core and cladding (blue line) over time.

Optics EXPRESS

The effect of this differential pressure and subsequent GDRI on the loss of the fiber modes was modelled using a commercial finite element solver (COMSOL Multiphysics). Assuming the initial gas pressure to be 18 kPa in the as-drawn fiber sample and using the one-dimensional pressure driven flow model described above, the longitudinal pressure distribution was calculated at equally spaced time steps between 0 and 20 hours. The refractive index profile of the air within the fiber at each time step was calculated using data from [22]. The modes in the associated fiber geometry are solved at a wavelength of 700 nm, a region within the window where the fiber guides with low loss. The loss as a function of axial position along the fiber core and time is shown in the two-dimensional map in Fig. 3(a). Modelling indicates that the attenuation along the fibre is not uniform for the first 15 hours. In fact, when examining the spatial loss distribution for the fundamental mode at three select times, as shown in the upper plot of Fig. 3(b), at 1.5 hours when the differential pressure between the core and capillaries is the greatest, the reduction in confinement loss is around 15 dB/km at a localized point halfway along the fiber. Similarly, for the HOMs also, Fig. 3(b) (lower) shows a reduction in loss of around 300 dB/km for the LP_{11} mode 1.5 hours after opening the fiber ends up to atmosphere. Figure 3(c) shows the total loss integrated over the fiber length as a function of time (fundamental mode only) indicating a maximum reduction in loss of 0.35 dB at 700 nm for our 36.75 m length fiber sample.

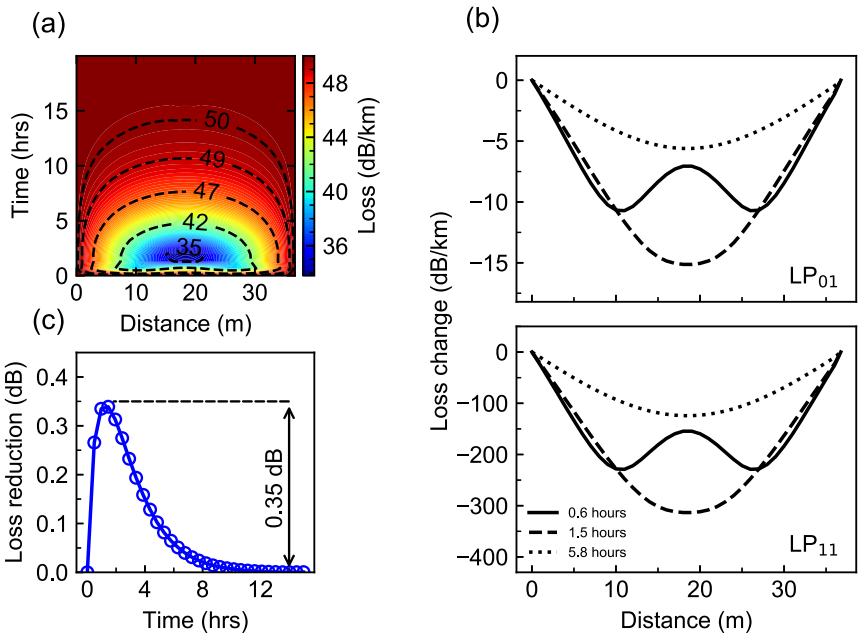

Fig. 3. (a) Simulated loss along a 36.75 m length of tubular HC-ARF as a function of time; (b) Simulated change in loss as a function of fiber length for the LP_{01} (top panel) and LP_{11} (lower panel) spatial modes at three different times after opening the fiber's ends to atmospheric pressure; (c) Integrated reduction in LP_{01} loss as a function of time.

3. Optical transmission measurements with as-drawn samples

Here, we perform experimental measurements on two different 'as-drawn' fiber samples. The first sample, as shown in Fig. 1(a), is 36.75 m in length and is the subject of the modelling study described in the previous section due to its simple geometry. The second sample is a 100 m length of NANF fiber that has a more complex microstructure geometry. The surrounding cylindrical membranes contain an additional nested anti-resonant element which significantly

Optics EXPRESS

reduces the optical loss and provides a HOM stripping mechanism [23]. In between fabrication and measurements, the fibers were kept within the laboratory with both ends sealed in order to maintain the as-drawn condition.

3.1. Tubular HC-ARF

For the tubular fiber, we periodically measured the transmission after exposing its internal microstructure to atmospheric pressure. The experimental set-up used to take broadband measurements is shown in Fig. 4(a). Prior to starting the measurement, the tubular fiber was in the 'as-drawn' condition described in Section 2, i.e., both ends of this fiber were sealed using a fusion splicer straight after fabrication. At the start of this experiment, the sealed fiber ends were cleaved thus exposing the internal microstructure to atmospheric pressure. One end of the fiber was then directly connected to a white light source (WLS, Bentham WLS100) using a bare fiber adapter (BFA). The output end of the fiber was then connected to an optical spectrum analyzer (OSA, Yokogawa AQ-6315A). Note that despite being directly connected to the WLS and OSA, the fiber ends are still open to atmospheric air. The experimental set-up was deliberately kept simple in order to minimize the impact of any drifts in optical alignment; this also enabled data acquisition to start promptly (2.4 minutes) after cleaving the fiber ends. An OSA trace was acquired every 1.5 minutes over a 21 hour period.

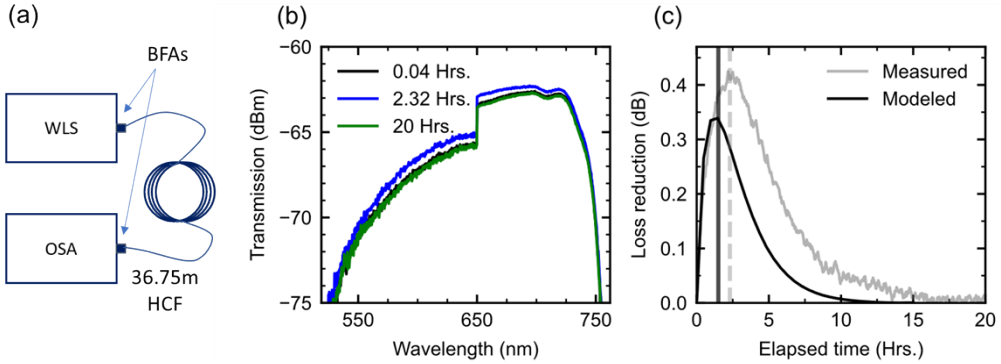

Fig. 4. (a) Experimental set-up used to monitor the transmission through a tubular HC-ARF over time. WLS: white light source; OSA: optical spectrum analyzer; BFAs: bare fiber adaptors; (b) Transmission spectrum recorded 2.4 minutes (black line), 2.32 hours (blue line) and 20 hours (green line) after opening the fiber ends to atmospheric pressure; (c) Measured change in loss over time at 700 nm wavelength (grey line) as compared to COMSOL simulations (black line) from Fig. 3(c).

The transmission spectra recorded at the start of the experiment (0.04 hours) and 2.32 hours after opening the ends are shown in Fig. 4(b) and the change in loss over the duration of the experiment at a wavelength of 700 nm is shown in Fig. 4(c). Note that the step feature in the traces in Fig. 4(b) at 650 nm wavelength is an artefact from the OSA data collection process (corresponding to a transition between gratings). Figure 4(b) shows that the transmitted power across the fiber's visible transmission window changed over the duration of the experiment. From Fig. 4(c), the time-dependence of this behavior is highlighted; we see that at a wavelength of 700 nm, the transmitted power initially increased, reached a maximum at a time of ~2.3 hours, before gradually reducing again and returning to approximately the same transmitted power at the start of the experiment after ~15 hours.

In Fig. 4(c), the experimental data is directly compared to the COMSOL modelling shown in Fig. 3(c) for 700 nm wavelength. We see that the general trend in both the modelling and experiment is very similar; initially the loss quickly reduces, and then it returns to its initial

Optics EXPRESS

value at a slower rate. However, there are small discrepancies between the modelling and experiment in terms of the time taken for maximum loss reduction (1.5 hours compared to 2.3 hours respectively) and the absolute maximum loss change. For the time taken, this discrepancy could be due to uncertainty in the precise initial as-drawn pressure inside the fiber, here we have assumed this to be 18 kPa based on the temperature drop in fabrication, but this is just an estimation. Furthermore, the gas flow model approximates the core to be a cylindrical channel; it has been shown that the spacing between the capillaries causes a drop in the average gas flow velocity in the core which increases the filling time [20], which could explain the longer time taken experimentally. For the absolute maximum loss change, it is important to note that the modelling only includes the fundamental mode; due to the coupling conditions used in this experiment, it is likely that there was some additional higher order mode content which, based on the LP_{11} mode modelling in Fig. 3(b), would explain why the measured loss change is higher than the modelled loss change considering the fundamental mode alone. Nevertheless, the general agreement between the experiment and modelling results support the notion that the low as-drawn pressure, and subsequent pressure-driven flow of surrounding air into the HCF after fabrication, leads to transient changes in the confinement loss.

For completeness, it is worth noting that at shorter wavelengths the experimentally measured change in transmission is higher (~0.6 to 0.8 dB in the wavelength range between 525 and 650 nm). While an increased sensitivity to GDRI is anticipated at shorter wavelengths, due to the smaller difference between the effective index of the core and cladding tubes, the experimentally measured changes at shorter wavelengths are higher than predicted by the simulations. For example, a maximum loss change of ~ 0.44 dB is predicted at a wavelength of 575 nm. While the data measured in the experiment is noisier in this wavelength range (due to a detector change within the OSA) which makes a comparison more difficult, this disagreement may also be partly due again to the simulated loss only considering the fundamental mode and also due to higher microbend sensitivity at shorter wavelengths, which is not accounted for in the simulations.

To investigate these transient loss changes further, an additional experiment was carried out. A second tubular fiber sample (with the same internal microstructure and similar in length to the first experiment) was prepared in a different manner; here just the cladding holes were sealed after the draw with the core left open to atmospheric pressure. The fiber was left in the laboratory for a period of two weeks to allow the core to equalize with atmospheric pressure. We then repeated the previous experiment; the experiment started when the two fiber ends were cleaved (opening up the cladding holes to atmospheric pressure) and the fiber was connected to the WLS and OSA. The evolution of the fiber's transmission spectrum was recorded over time and the transmission spectra recorded during this additional experiment are shown in Fig. 5(a). Figure 5(a) shows that the loss of the fiber increases across the entire transmission window as a function of time. This is due to the changing (increasing) internal pressure in the cladding tubes which increases the effective indices of the modes that reside in these tubes. This results in a decrease in the difference between the effective indices of the core and cladding modes which leads to the increasing loss. Figure 5(b) shows the increase in loss with time at three select wavelengths across the visible band (620, 650, 750 nm). After ~15 hours, the transmission stabilizes; this corresponds to the time at which the cladding hole pressure is expected to have equalized with the surrounding atmospheric pressure (see modelling in Fig. 2(b)) and therefore provides further evidence that the combination of low initial gas pressure inside a HCF and subsequent pressure driven gas flow can lead to transient changes in the optical properties of the fiber.

3.2. Nested nodeless anti-resonant fiber (NANF)

Here, a further experiment is carried out with an as-drawn fiber sample that has a more complex microstructure involving multiple reflective glass membranes, similar to recent state of the art low loss fibers including NANFs [4] and conjoined tube fibers [17]. This section will focus on

Optics EXPRESS

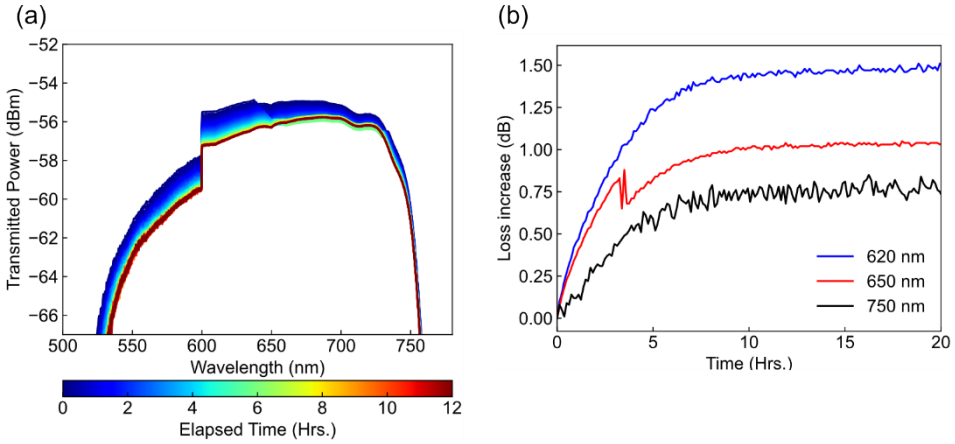

Fig. 5. (a) Transmission spectra recorded throughout the duration of the experiment (step at 600 nm due to change in grating in the OSA). (b) Measured change in loss at three selected wavelengths: 620, 650 and 750 nm. Note that the step feature in the red trace (for 650 nm wavelength) is an artefact from the OSA data collection process.

the NANF design which has losses approaching that of standard optical fibers [4]. This fiber geometry has a more complex cladding microstructure with an additional set of nested tubes with the same thickness as the outer ones therefore different selective pressure differentials are applied to the preform during the draw in-line with fluid dynamics modelling [16]. For this reason, the as-drawn pressure of the NANF will differ from the tubular structure.

An SEM of the fiber measured is shown in Fig. 6(a). For this experiment the NANF used was 100 m in length. It has a core diameter of 31.7 μm and a cladding structure which consists of outer and inner tubular elements with diameters of 30.9 and 13.1 μm respectively. As with the first experiment on tubular HC-ARF, both ends of this fiber were sealed immediately after fabrication to preserve the as-drawn condition. The experimental setup is similar to that in Fig. 4(a) except that the input end of the NANF is hermetically spliced to a large mode area (LMA) all-solid fiber. The splicing process took around 1.5 minutes, during which, one end of the NANF was open to atmospheric pressure (the other end remained sealed). The spliced end of the NANF was connected to the WLS (again, Bentham WLS100) via a single-mode fiber (SMF) patch-cord. The output end of the NANF was connected to the OSA using a BFA. This simple setup ensures stable and consistent coupling conditions. In this configuration, only one end of the fiber is open to atmospheric pressure during the experiment.

Figure 6(b) shows the transmission spectrum recorded through the NANF at the start of the experiment, 0.08 hours after cleaving the output end and at 15.6 and 71 hours. As can be seen, the short wavelength edge position moves significantly during the as-drawn re-pressurisation process - shifting towards the shorter wavelength direction by ~24 nm when comparing the traces at 0.08 hours and 15.6 hours. Note, the feature seen at ~1.35 μm is an absorption feature, attributed to the ingress of atmospheric water vapour. Figure 6(c) shows the transmission over time for three selected wavelengths. Near the shorter wavelength edge of the transmission window, the transmitted power initially increases, reaches a maximum at ~15.6 hours after opening the fiber end, and then gradually reduces until at ~60 hours after unsealing the fiber end, the transmission stabilizes. This general transmission trend observed for the NANF is similar to that observed with the tubular HC-ARF but there are a couple of notable differences.

Firstly, the time before the maximum power was reached and the time for the power stabilization are both notably longer; this is due to the longer fiber length used, the fiber's more complex

Optics EXPRESS

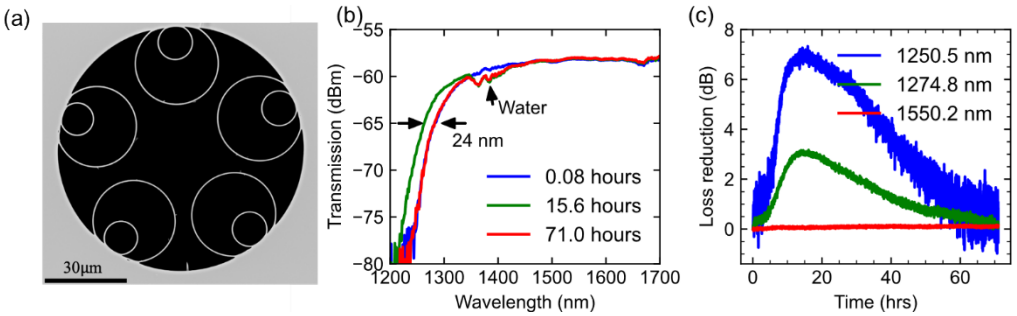

Fig. 6. (a) SEM image of the 5-tube NANF used in this experiment; (b) Transmission spectra through the 100 m NANF 4.8 minutes (blue line), 15.6 hours (orange line) and 71 hours (red line) after cleaving the as-drawn NANF; (c) Change in power recorded at three different wavelengths through the 100 m NANF sample as a function of time after opening the ends of the fiber to atmospheric pressure.

geometry, and that it was only opened to atmosphere at one end. Secondly, the transmission change is more localized to shorter wavelengths and at 1550 nm wavelength, no noticeable change was recorded. This can be attributed to a combination of two factors. As mentioned earlier, at shorter wavelengths the effective indices of the core and cladding modes are closer, so that modifications in the effective indices of these regions due to GDRI have a more significant impact on the fiber's optical properties. Additionally, close to the short wavelength edge of the transmission window, the confinement loss of the fiber rapidly increases with decreasing wavelength; this also makes this spectral region especially sensitive to GDRI and here this is clearly seen as the short wavelength edge shifts by up to 24 nm at a time 15.6 hours into the measurement. At longer wavelengths, away from the short wavelength edge, the confinement loss of this NANF design is extremely low, < 0.5 dB/km [24], which means the absolute change in loss due to GDRI is small and more challenging to measure with this experimental set up and the 100 m fiber length used. The short wavelength edge of the fundamental transmission window reverts back to its initial position 71 hours after exposing the fiber to atmospheric pressure. If this shift were due to pressure-induced changes in the fiber air region's refractive index altering the resonance condition of the membranes, a permanent and irreversible alteration would be expected, which is not observed.

4. Discussion

To put these results in context, it is useful to consider the implications through HCF design, fabrication processes, characterization and to ultimately consider the impact on different applications in different deployment conditions. From the fiber design perspective, the magnitude of the transient changes in optical performance will depend on both the fiber geometry and the operating wavelength, as evidenced by the differences in the behavior of the tubular and NANF designs investigated in this work. The fiber geometry is also critical from a gas flow perspective. From [18], the gas filling time in a cylindrical tube scales as

$$t_{fill} \propto \left(\frac{L}{2r}\right)^2 \tag{2}$$

where L is the fiber length and r is the hole radius. It is important to consider that in this respect, the smallest element in the fiber's cross-sectional geometry will be the limiting factor in terms of the timescales required for pressure equalization (and thus, stabilization of the optical performance). This smallest element will usually be in the cladding of the HCF and can vary in

Optics EXPRESS

diameter from between a few μm to several tens of μm, depending on fiber design and operating wavelength range. As an example, if we consider a 500 m length of a HCF with 6 μm diameter cladding holes (which could be the case for a 10-element visible-guiding tubular fiber), the estimated filling time for the cladding features, based on an initial pressure of 18 kPa would be ~6 months. Furthermore, as the filling time also scales with the square of the fiber length, if this 500 m length was doubled to a 1 km length, the expected filling time would increase by a factor of 4. These timescales only represent an estimation, as the model in [18] only considers gas flow in an idealized circular hole and is validated on short fiber lengths and thus further work is required to measure gas filling times in longer fibers. Nevertheless, this serves to highlight that the transmission of a HCF could change post-fabrication over a prolonged period, which will be substantially extended by long fiber lengths and small cladding features.

The fiber treatment and storage post-fabrication will determine whether this pressure equalization starts straight after fabrication (in the case that the fiber ends are left open within an atmospheric environment) or later (if the ends are initially sealed). HCF characterization, for example via the cutback technique, is often carried out with the fiber ends open to the surrounding atmospheric gases and can take around 1-2 hours to complete. As evident from the experimental results reported here, and the discussion regarding the impact of fiber geometry and length, the changes in the transmission over this time period could vary substantially, from being negligible to very significant. For the tubular HCF discussed in this manuscript, the loss was experimentally determined by cutback measurement to be 46 dB/km at a wavelength of 700 nm. For the 36.75 m length used here, this loss value would imply a ~1.7 dB insertion loss. According to Fig. 4(c), the maximum transient change observed at this wavelength was ~0.4 dB, which would reduce the recorded insertion loss to 1.3 dB, and lead to a cutback loss estimation of ~35 dB/km. Estimating the impact on a cutback loss measurement is not straightforward, as there would be a pressure profile along the fiber, and a wavelength dependence. However, this example does highlight that transient changes of the magnitude recorded would impact the cutback loss estimation and therefore could lead to inaccurate characterization.

Beyond characterization, the potential impact of GDRI driven transmission changes will depend on the application and fiber deployment scenario. For some applications, the fiber could be hermetically sealed, for example, when fusion spliced to a conventional fiber. In this scenario, the internal gas pressure is isolated from the environment, and, after the pressure profile inside the fiber has stabilized along the fiber length, there should not be any transmission changes due to transient GDRI. This should apply even if the core and cladding pressure are not equal, assuming no gas permeation between these different regions. However, if the core and cladding pressure are not equal with the surrounding environment's gas pressure, the potential for GDRI-driven transmission changes should be considered if the hermetic seal is then broken, due to subsequent pressure-driven gas ingress. For applications where the fiber will be used with open ends, for example in sensing, then pre-equalization of the core and cladding pressures will eliminate any transmission changes due to transient GDRI, though again it is worth noting that the timescales to achieve this are not insignificant for longer fiber lengths.

As a final note, here we have primarily focused on discussing the change in the fiber loss exemplified by the changes in transmitted power through a HCF which are due to the initial sub-atmospheric pressure and subsequent transient GDRI. While a GDRI in a HCF acts to change the attenuation of the fiber through changing the confinement loss and bend loss [15], it is important to note that these changes not only apply to the fundamental mode of the HCF, but that the modality of the fiber will also likely change during the transient period which could be important depending on the characterization method or application.

Optics EXPRESS

5. Conclusion

In this work, we have investigated the stability of the transmission of as-drawn HCFs. These as-drawn HCFs are fibers which are sealed immediately after fabrication in order to preserve the initial gas composition and pressure within the core and cladding elements of the fiber. Experimental results on both tubular HCFs and NANFs have shown transient changes in the fiber transmission when the ends of the fibers are cleaved and atmospheric gas species (at s.t.p.) enter the core and cladding elements of the HCF due to the pressure difference between the voids inside the fiber and the surrounding atmosphere. For both fiber designs, similar trends in the transmission changes are observed; the transmitted power increases and then gradually returns to approximately the initial level. This highlights that sub-atmospheric initial pressure and GDRI impacts the transmission of a range of HC-ARF designs. As the fiber length is increased, the timescales over which these effects occur will become significantly longer. The presented data also highlights a wavelength dependence in the transmission changes, with larger changes being observed at shorter wavelengths.

To understand the origin of these changes, both gas flow simulations and optical modelling were carried out. By approximating the initial gas pressure inside the fiber as 18 kPa and simulating the increase in internal gas pressure along a tubular HCF as a function of length, we could estimate the timescales required for the gas pressure inside a 36.75 m fiber length to equalize with the surrounding atmospheric gas pressure for both the core and cladding elements of the fiber. Comparing these simulations to the experimental changes in transmission, we observed similar evolutions of change in loss as a function of time, indicating that this differential pressure plays a role in the transient changes. Similar agreements were achieved by isolating the impact of the gas flow into the cladding elements only, where gas in the core region had already equalized with atmospheric pressure. Moreover, we observe the same consistency in behavior in a more complex, NANF, design. This agreement, along with COMSOL simulations on the optical performance of the tubular HCF with differential core and cladding pressure, strongly support the hypothesis that a transient GDRI between the core and cladding elements of the HCFs, driven by the initial sub-atmospheric internal gas pressure, is fueling these transient changes in optical performance. As such, the timescales over which these changes occur depend on fiber design, whether both ends of the fiber are open to atmosphere and the fiber length [18]. These transient changes in the optical properties of HCFs, driven by gas flow dynamics, are important to consider for accurate characterization of HCFs as well as in fiber deployment, where consistent optical performance is critical.

Funding. Engineering and Physical Sciences Research Council (EP/N00762X/1, EP/P030181/1).

Disclosures. The authors declare that there are no conflicts of interest related to this article.

Data availability. All data supporting this study are available from the University of Southampton repository at [25].

References

1. G. T. Jasion, T. D. Bradley, H. Sakr, *et al.*, "Recent breakthroughs in hollow core fiber technology," Proc. SPIE **11309**, 1 (2020).
2. R. Mears, K. Harrington, W. J. Wadsworth, *et al.*, "Guidance of ultraviolet light down to 190 nm in a hollow-core optical fibre," Opt. Express **32**(6), 8520–8526 (2024).
3. J. H. Osório, F. Amrani, F. Delahaye, *et al.*, "Hollow-core fibers with reduced surface roughness and ultralow loss in the short-wavelength range," Nat. Commun. **14**(1), 1146 (2023).
4. H. Sakr, Y. Chen, G. T. Jasion, *et al.*, "Hollow core optical fibers with comparable attenuation to silica fibers between 600 and 1100 nm," Nat. Commun. **11**(1), 6030 (2020).
5. F. Yu, P. Song, D. Wu, *et al.*, "Attenuation limit of silica-based hollow-core fiber at mid-IR wavelengths," APL Photonics **4**(8), 080803 (2019).
6. G. T. Jasion, H. Sakr, J. R. Hayes, *et al.*, "0.174 dB/km Hollow Core Double Nested Antiresonant Nodeless Fiber (DNANF)," in *Optical Fiber Communications Conference and Exhibition* (2022), pp. 1–3.
7. B. J. Mangan, B. Zhu, G. S. Puc, *et al.*, "Low latency transmission in a hollow core fiber cable," *Conference on Lasers and Electro-Optics* (2021), pp. 1–2.

Optics EXPRESS

8. euNetworks Fiber U.K. Limited, "euNetworks deploys Lumenisity limited coresmart hollow core fibre cable in London," euNetw. Fiber U.K. Ltd., London, UK, Apr. 14, 2021. [Online]. Available: https://eunetworks.com/app/uploads/2021/04/euNetworks-deploys-Lumenisity-Hollowcore-Fibre-in-London-FINAL.pdf
9. S. Rikimi, Y. Chen, T. D. Bradley, *et al.*, "Comparison between the Optical Performance of Photonic Bandgap and Antiresonant Hollow Core Fibers after Long-Term Exposure to the Atmosphere," in *Optical Fiber Communications Conference and Exhibition* (2022), pp. 1–3
10. B. Debord, F. Amrani, L. Vincetti, *et al.*, "Hollow-core fiber technology: the rising of gas photonics," Fibers **7**(2), 16 (2019).
11. N. V. Wheeler, M. N. Petrovich, N. K. Baddela, *et al.*, "Gas absorption between 1.8 and 2.1 μm in low loss (5.2 dB/km) HC-PBGF," in *CLEO* (Optical Society of America, 2012), paper CM3N.5.
12. J. K. Lyngsø, B. J. Mangan, C. Jakobsen, *et al.*, "7-cell core hollow-core photonic crystal fibers with low loss in the spectral region around 2 μm," Opt. Express **17**(26), 23468–23473 (2009).
13. S. Rikimi, Y. Chen, M.C. Partridge, *et al.*, "Pressure in as-drawn hollow core fibers, in *Advanced Photonics Congress*, paper SoW1 H.4 (2020).
14. S. Rikimi, Y. Chen, T. W. Kelly, *et al.*, "Internal gas composition and pressure in as-drawn hollow core optical fibers," J. Lightwave Technol. **40**(14), 4776–4785 (2022).
15. T. W. Kelly, P. Horak, I. A. Davidson, *et al.*, "Gas-induced differential refractive index enhanced guidance in hollow-core optical fibers," Optica **8**(6), 916–920 (2021).
16. Gregory T. Jasion, John R. Hayes, Natalie V. Wheeler, *et al.*, "Fabrication of tubular anti-resonant hollow core fibers: modelling, draw dynamics and process optimization," Opt. Express **27**(15), 20567–20582 (2019).
17. S. F. Gao, Y. Y. Wang, W. Ding, *et al.*, "Hollow-core conjoined-tube negative-curvature fibre with ultralow loss," Nat. Commun. **9**(1), 2828 (2018).
18. J. Henningsen and J. Hald, "Dynamics of gas flow in hollow core photonic bandgap fibers," Appl. Opt. **47**(15), 2790–2797 (2008).
19. R. Wynne and B. Barabadi, "Gas-filling dynamics of a hollow-core photonic bandgap fiber for nonvacuum conditions," Appl. Opt. **54**(7), 1751–1757 (2015).
20. P. Bojęś, P. Jaworski, K. Krzempek, *et al.*, "Experimental and numerical analysis of gas flow in nodeless antiresonant hollow-core fibers for optimization of laser gas spectroscopy sensors," Opt. Laser Technol. **152**, 108157 (2022).
21. J. A. Bearden, "A precision determination of the viscosity of air," Phys. Rev. **56**(10), 1023–1040 (1939).
22. A. Börzsönyi, Z. Heiner, M. P. Kalashnikov, *et al.*, "Dispersion measurement of inert gases and gas mixtures at 800 nm," Appl. Opt. **47**(27), 4856–4863 (2008).
23. F. Poletti, "Nested antiresonant nodeless hollow core fiber," Opt. Express **22**(20), 23807–23828 (2014).
24. H. Sakr, T. D. Bradley, G. T. Jasion, *et al.*, "Hollow core NANFs with five nested tubes and record low loss at 850, 1060, 1300 and 1625 nm," in *Optical Fiber Communications Conference and Exhibition* (2021), pp. 1–3.
25. T.W. Kelly, S. Rikimi, I.A. Davidson, *et al.*, "Dataset for Transient Gas-induced Differential Refractive Index Effects in As-drawn Hollow Core Optical Fibers," University of Southampton (2024), http://dx.doi.org/10.5258/SOTON/D3051.